Biomaterials Science

ROYAL SOCIETY OF CHEMISTRY

PAPER

View Article Online
View Journal | View Issue

Cite this: *Biomater. Sci.*, 2022, **10**, 1981

Investigation and comparison of resin materials in transparent DLP-printing for application in cell culture and organs-on-a-chip†

Anna Fritschen, *[a] Alena K. Bell, [b] Inga Königstein, [a] Lukas Stühn, [b] Robert W. Stark[b] and Andreas Blaeser*[a,c]

Organs-on-a-Chip (OOCs) have recently led to major discoveries and a better understanding of 3D cell organization, cell–cell interactions and tissue response to drugs and biological cues. However, their complexity and variability are still limited by the available fabrication technology. Transparent, cytocompatible and high-resolution 3D-printing could overcome these limitations, offering a flexible and low-cost alternative to soft lithography. Many advances have been made in stereolithography printing regarding resin formulation and the general printing process, but a systematic analysis of the printing process steps, employed resins and post-treatment procedures with a strong focus on the requirements in OOCs is missing. To fill this gap, this work provides an in-depth analysis of three different resin systems in comparison to polystyrene (PS) and poly(dimethylsiloxane) (PDMS), which can be considered the gold-standards in cell culture and microfluidics. The resins were characterized with respect to transparency, cytocompatibility and print resolution. These properties are not only governed by the resin composition, but additionally by the post-treatment procedure. The investigation of the mechanical (elastic modulus ~2.2 GPa) and wetting properties (~60° native / 20° plasma treated) showed a behavior very similar to PS. In addition, the absorbance of small molecules was two orders of magnitude lower in the applied resins (diffusion constant ~0.01 $\mu m^2\ s^{-1}$) than for PDMS (2.5 $\mu m^2\ s^{-1}$), demonstrating the intrinsic suitability of these materials for OOCs. Raman spectroscopy and UV/VIS spectrophotometry revealed that post-treatment increased monomer conversion up to 2 times and removed photo initiator residues, leading to an increased transparency of up to 50% and up to 10-times higher cell viability. High magnification fluorescence imaging of HUVECs and L929 cells cultivated on printed dishes shows the high optical qualities of prints fabricated by the Digital Light Processing (DLP) printer. Finally, components of microfluidic chips such as high-aspect ratio pillars and holes with a diameter of 50 µm were printed. Concluding, the suitability of DLP-printing for OOCs was demonstrated by filling a printed chip with a cell–hydrogel mixture using a microvalve bioprinter, followed by the successful cultivation under perfusion. Our results highlight that DLP-printing has matured into a robust fabrication technology ready for application in extensive and versatile OOC research.

Received 23rd November 2021,
Accepted 23rd February 2022

DOI: 10.1039/d1bm01794b

rsc.li/biomaterials-science

1. Introduction

Microfluidic devices today are commonly used in biomedical research such as cancer research,[1] *in vitro* bio-assays,[2] drug delivery[3] or fundamental research on cell behavior,[4] as they offer a precise realistic microenvironment for cells.[5] Their application in Organs-on-a-Chip (OOCs) has become of greatest interest in the community, as they offer a highly biomimetic environment by including media flow conditions and allow for the combination of multiple organ models. Additionally, nutrient and drug supply as well as pharmacokinetic read-outs is improved compared to static culture condition.[6,7]

Today, these devices are commonly produced by soft-lithography and PDMS molding, which is a time-consuming process and lacks flexibility.[5] As an alternative, additive manufacturing has recently emerged as a versatile and flexible

[a]*Technical University of Darmstadt, Department of Mechanical Engineering, BioMedical Printing Technology, Magdalenenstr. 2, 64289 Darmstadt, Germany. E-mail: fritschen@idd.tu-darmstadt.de, blaeser@idd.tu-darmstadt.de*
[b]*Technical University of Darmstadt, Institute of Materials Science, Physics of Surfaces, Alarich-Weiss-Str. 16, 64287 Darmstadt, Germany*
[c]*Technical University of Darmstadt, Centre for Synthetic Biology, Schnittspahnstr. 10, 64287 Darmstadt, Germany*

†Electronic supplementary information (ESI) available. See DOI: 10.1039/d1bm01794b

technology for cell biology applications such as tissue engineering and biomedical research.[8,9] Stereolithography (SL) printing has been proven to fulfil the requirements of OOC research – high transparency, cytocompatibility and high resolution – while offering a greater freedom of design and high potential for rapid prototyping.[10]

The most frequently applied resins for transparent SL-printing include poly(ethylene glycol) diacrylate (PEG-DA),[11–16] a PETA/HAD mixture,[17] poly(dimethylsiloxane) (PDMS),[18] poly (caprolactone) methacrylate,[19] VisiJet's SL Clear resin,[20] Asiga's PlasCLEAR[21] and a Pro3dure's GR-10 methacrylate based resin.[22] To fabricate channels, holes or spacers small enough to fulfil the requirements for biomimetic OOC systems,[3,13,15] tailoring the printing process as well as the photo initiator and sensitizer system are crucial.[11] Besides its physical properties, in the context of OOCs the cytocompatibility of the material system is of particular interest. The latter has proven to be challenging as the applied resins commonly comprise toxic monomers, such as acrylates, methacrylates or urethanes.[2,23] Still, extensive post-treatment with UV-light was shown to significantly reduce their toxicity potential.[24] Recent studies shed light on the printing of transparent and cytocompatible microfluidic devices,[11,13,14,18] or the application of 3D-printing technology for the fabrication of molds or accessories.[3,25,26] Albeit crucial for the rapid-prototyping of transparent and cytocompatible OOCs, so far a systematic evaluation of the material systems as well as the printing process and the post-fabrication treatment of printed parts is missing.

This paper addresses this challenge and presents a comprehensive analysis of the complex interplay of material systems and printing process for the rapid-prototyping of OOCs. Three resin material systems were thoroughly studied and compared to two standard cell culture and microfluidic materials, PDMS and polystyrene (PS). The resins include a commercial resin from Asiga named PlasCLEAR, poly(ethylene glycol) diacrylate (PEG-DA) mixed with a photo initiator and PEG-DA mixed with both an initiator and a sensitizer. The article highlights the strengths and weaknesses of the three material compositions regarding printability, optical and mechanical properties, absorbance of small hydrophobic molecules and proteins, suitability for high resolution imaging and fluorescence microscopy as well as their cytocompatibility. Our study shows that the requirements of transparency, cytocompatibility and printing resolution can be adequately addressed by modifying the printing hardware (*e.g.* printing platform), the resin formulation (*e.g.* photo initiator and sensitizer), and by applying dedicated post-fabrication treatments (*e.g.* UV exposure, solvent extraction).

Finally, to demonstrate that the technology and method of transparent Digital Light Projection (DLP)-printing is ready for routine application, we fabricated a complete microfluidic chip designed for OOC culture. This chip was filled using a commercial 3D-bioprinter with a cell–hydrogel mixture and the demonstrator was successful under perfusion for multiple days.

2. Results and discussion

2.1. Hardware modifications

Considerations and preparations for transparent SL-printing do not only concern the selection of a suitable raw material, but the printer's hardware itself influences the transparency of the resulting parts. Critical components of a standard printer based on a Digital Light Projector (DLP-printer) are the vat containing the resin and the build plate, onto which the printed part attaches to (Fig. 1A). In the printed parts, light scattering occurs on surface roughness and bulk defects caused by scratches in the build plate and resin vat of the printer. This diffuse scattering significantly reduces the transparency of prints (Fig. 1C). The printer's original build plate was therefore replaced by a highly polished and hardened steel plate, and a siliconized glass Petri dish was used as resin vat[11,13] (Fig. 1B). Confocal laser scanning microscopy (CLSM) images show the significant reduction of surface roughness from 1.34 μm R_a value (original build plate), to 5 nm R_a value (modified set-up), which is comparable to the roughness of glass microscopy slides (Fig. 1D).

2.2. Material selection

Materials employed in transparent and cytocompatible SL-printing are usually made of an acrylate-based monomer. The monomer is cured by a photo initiator that starts a radical polymerization process under light exposure.[23] By adding type II initiators that react as photo sensitizers the print resolution is further improved.[27] Commercial resins can contain additional stabilizers, fillers and plasticizers to optimize print behavior.[2]

SL resins have to fulfil certain requirements that can be classified into three categories. (1) Regarding optical properties, they have to absorb light at the DLP wavelength of the printer, usually between 380 and 410 nm,[28] while being completely transparent after printing in the range of visible and near UV light (350–800 nm) for application in light and fluorescence microscopy. (2) In terms of printability, a good spatial resolution of the crosslinking reaction is key for OOC applications to create high-aspect ratio prints as well as open microfluidic channels. (3) For application in cell culture and OOC, the printed parts need to exhibit long-term cytocompatibility. In particular, this is important since the radical forming type I photo initiators as well as the acrylate-based monomers are toxic by nature.[24,29,45] However, previous works could show that solvent extraction as well as prolonged UV exposure times after printing greatly reduce cytotoxicity. During the prolonged post-treatment, photo initiator residues can be reduced, as shown for cell culture and zebrafish embryos.[20,24,29]

In our work, we chose to compare three different resin compositions regarding their suitability for printed microfluidic devices for cell culture applications. The selection was based on their optical properties as well as their previous use in cytocompatible and transparent SL-printing. The commercial PlasCLEAR resin by the printer's manufacturer is based on diurethane dimethacrylate and tetrahydrofuryl methacrylate.[30]

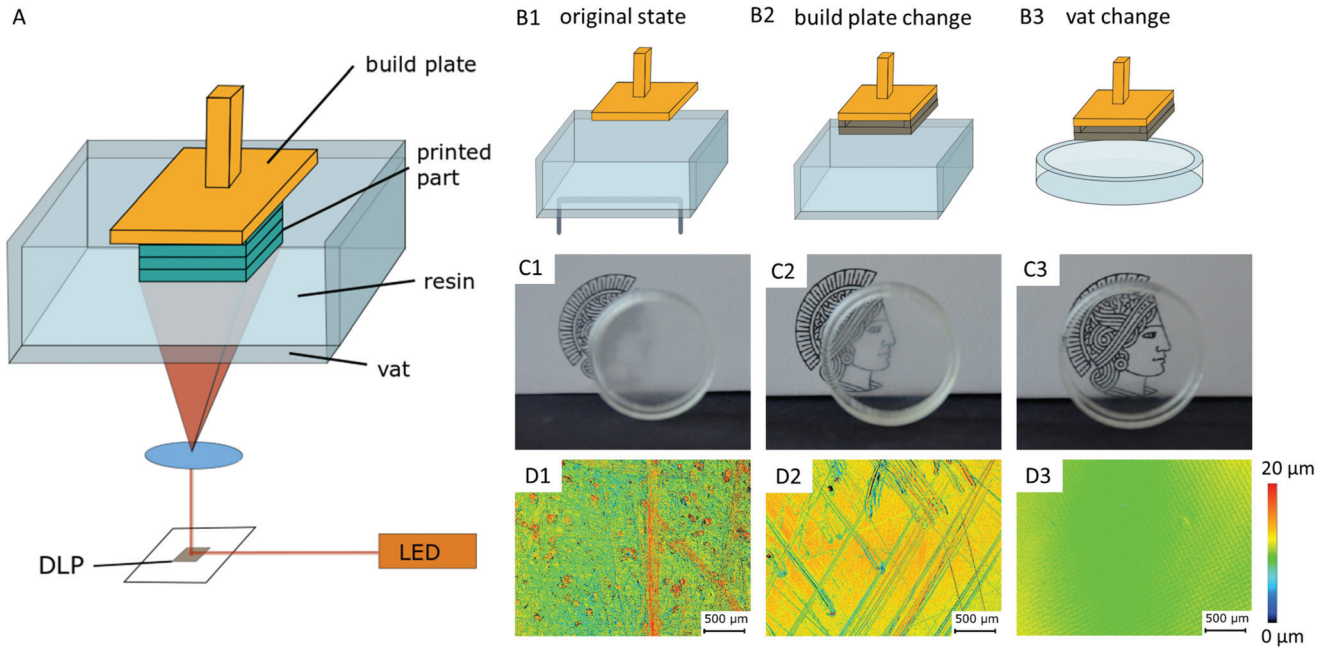

Fig. 1 General concept of DLP-printing shown for the Asiga Pico 2^{HD} 27 printer. The print image is projected into a resin-containing vat by a Digital Light Projector (DLP), causing a layer of resin to become cured and to attach onto the build plate (A). Modifications of the printer from its original state include a change of build plate and vat (B), which leads to an increasing transparency in the resulting print (C) and a reduced surface roughness of the print as shown in surface topography images of side facing the build plate (D1) and vat (D2, 3).

The manufacturer customized the resin to fit the printer, and it has been shown to offer a good print resolution[21,22] as well as cytocompatibility with Chinese Hamster Ovary cells.[31]

To better control the influence of resin components on viability, printability and optical properties, two PEG-DA based compositions were mixed as well. The first one, named PEG-1, contains 0.4 wt/vol% BAPO as photo initiator, and the second one, PEG-2, additionally 0.1 wt/vol% ITX as photo sensitizer. We chose PEG-DA as a base material as it comprises a low non-specific molecule adsorption and bulk fluorescence,[32,33] high stability in water and other solvents typically used in cell culture[15] and overall better performance when compared to other diacrylates.[34] PEG-DA based materials have already been successfully printed on Asiga printers before[11,21] and were shown to be cytocompatible with various cell lines.[11,14] As an initiator system, BAPO exhibits a high print resolution when combined with PEG-DA[15,21,35] and good cytocompatibility after post-treatment when added at low concentrations.[11,16,29,34,36] The addition of ITX as photo sensitizer has been suggested to improve printing resolution while exhibiting good biocompatibility after post-treatment steps.[13,18] Compared to other groups, we decided to reduce the amount of BAPO[14,21] and ITX[13,35] to reduce possible cytotoxicity[29,36] and improve transparency.[34]

UV/VIS spectrophotometry reveals that all three compositions absorb light at the 385 nm printer wavelength and are therefore suitable for the system (Fig. 2A). Additionally, they are all transparent in the visible wavelength range (Fig. S1, ESI†), making them suitable for transparent printing of bio-

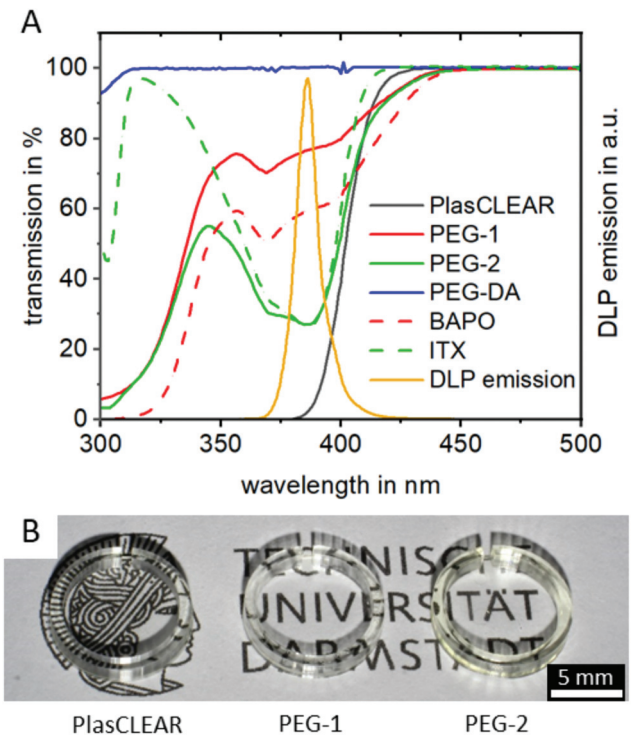

Fig. 2 UV/VIS photospectroscopy of all resins and their single components shows the transmission of light at wavelengths between 300 and 500 nm (left *y*-axis), with the printer's DLP emission spectrum (right *y*-axis) showing a clear peak at 385 nm (A). Images of printed cell culture dishes of all printing materials show the high post-printing transparency for all three selected resins (B).

compatible and microfluidic systems, as we could show by printing small cell culture dishes (Fig. 2B).

Adding the photo sensitizer ITX increases the absorbance of PEG-2 by a factor of two compared to PEG-1. We therefore expected an improved print resolution and reduced print times. The commercial PlasCLEAR resin exhibits the highest absorbance at wavelengths below 400 nm, which indicates an even better print resolution. At the same time, no light is transmitted at all at wavelengths below 400 nm for the PlasCLEAR resin. Considering the excitation wavelength of frequently applied fluorescent dyes that fall in this range, such as DAPI, the cut-off in transparency represents a challenge. In contrast, the applied PEG-DA based resins exhibit a high transmission at wavelengths between 330 and 400 nm. As such, they raise the expectation to be a promising solution for a broader range of UV-light excited fluorescent dyes.

2.3. General material comparison to PS and PDMS

Besides its transparency, the mechanical and wetting behavior of DLP-printed lab ware is crucial. In order to achieve results comparable to standard lab ware, both properties were assessed for components produced from the three described resins and compared to polystyrene (PS)-based materials, the gold-standard in tissue culture; and to PDMS, which is the most common material in microfluidic chips for cell culture.

All three acrylate-based materials show an elastic modulus of 2.3 to 2.4 GPa by nanoindentation after printing, which is comparable to that of PS and approximately 50 times higher than for PDMS (Fig. 3A). Cell behavior when cultured on these parts is therefore expected to be the same as for commercial, standard lab ware, as stiffness of substrate influences cell morphology, proliferation and differentiation.[37,38]

Hydrophilicity is another important factor in cell culture, especially for successful attachment of cells on the printed structures and also for optimal fluid flow inside of microfluidic channels. In their native state, all three materials show a contact angle with water between 60° and 70°, which is comparable to that of polystyrene and lower than for PDMS (Fig. 3B). Plasma treatment significantly reduces the contact angle to below 20°, which is comparable to glass or plasma-treated PS or PDMS. It therefore improves cell adhesion and wettability for long lasting cell adhesion without chemical surface treatment. This property is especially favorable for OOC, where stable endothelial lining of perfused channels is often desired, which is not possible with native PDMS.

As a hydrophobic material, PDMS is a problematic material in OOCs as it greatly absorbs small hydrophobic molecules and is prone to fouling when in contact with important cell culture proteins such as bovine serum albumin (BSA). The diffusivity of Nile Red (small lipophilic molecule) and FITC-labelled BSA in PDMS is with 1–2.5 $\mu m^2\ s^{-1}$ two to three orders of magnitude higher than in prints (Fig. 3C and D). The observed diffusivity is slightly higher in PlasCLEAR than in the PEG-based materials, which could correlate to the slightly higher hydrophobicity of the material in its native state (Fig. 3B). Since metabolic assays of protein expressions and general pharmacokinetic analyses are of key interest in OOCs, this greatly reduced absorbance of molecules of acrylates compared to PDMS renders them as a preferential material in OOCs.

2.4. Influence of post-treatment on cross-linking in prints

In DLP-printing, photo initiator residues and uncured monomer components remain in the cured material directly after the printing process. These residues are thought to impact biocompatibility and transparency of prints, as discussed later. For this reason, different post-treatment steps, such as UV-light exposure and solvent extraction, and their effect on improving monomer conversion were quantified using Raman spectroscopy. The studied post-treatment steps included overnight extraction in water, isopropanol (IPA) or no solvent, as well as 0, 4 or 8 hours of UV exposure in a water bath.

For all three materials, Raman detail spectra were taken in the fingerprint region from 1000 to 1800 cm^{-1}, where three important peaks could be identified. For PlasCLEAR, the peak

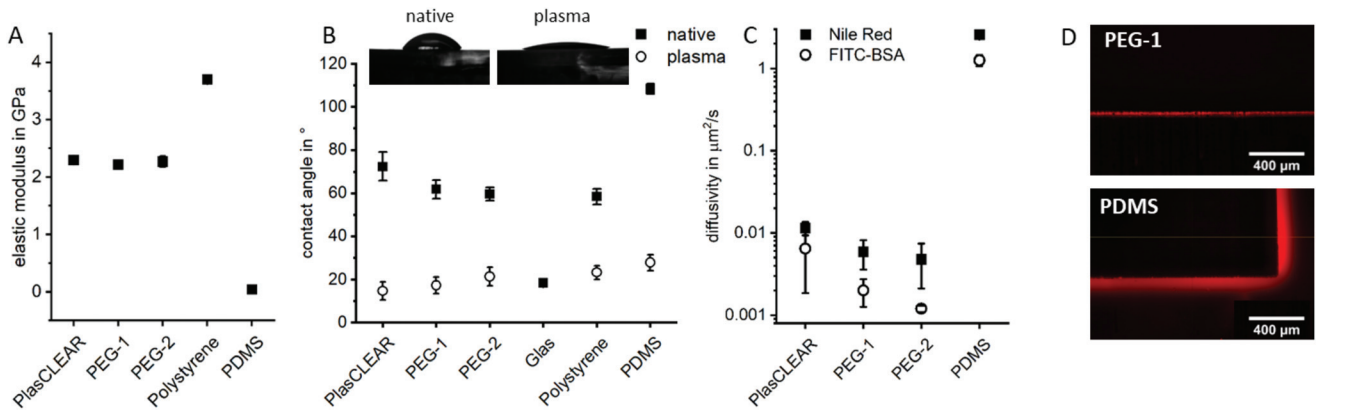

Fig. 3 Characterization of prints for their elastic modulus by nanoindentation (A) and their contact angle with water in their native state and after plasma treatment (B). The diffusivity of Nile Red and FITC-BSA (C) was determined by fitting the intensity of the fluorescent signal under the microscope (D) using Fick's 2nd law of diffusion.

ratio between the aliphatic C=C stretch of both the reactive monomer end groups and photo initiator groups at 1410 cm^{-1}, and the $-CH_2$ deformation mode at 1470 cm^{-1} can be taken as a measure for the amount of uncured resin[39] (Fig. 4A and D). The $-CH_2$ deformation mode signal is given by the cured acrylate backbone chain and stays largely constant once cured, while the amount of leftover reactive groups decreases with increasing conversion rate. The peak ratio of C=C stretch to $-CH_2$ deformation therefore also decreases with increasing conversion rate. A decreasing peak ratio is expected to result in a higher cytocompatibility for PlasCLEAR, as unwanted residual groups are less present in this case.

The Raman measurement reveals this decrease in reactive C=C bonds with post-treatment compared to the untreated sample (air, 0 h UV). A clear distinction between samples extracted in IPA overnight and other post-treatment is visible, with a 30% lower amount of reactive bonds left after extraction. For samples without solvent extraction, a slight decrease in C=C bonds with increasing UV exposure time is seen as well.

For both PEG-DA based resins, the emerging peaks between 1040 and 1140 cm^{-1}, corresponding to C–C stretching vibrations of linear and branched C–C bonds as well as various C–O–C bond modes in the polymer chain,[40,41] are taken for the degree of cross-linking, as the aliphatic C=C stretch signal is very weak (Fig. 4B and C). In case of these resins, an increase in the ratio of these bond modes compared to the predominantly constant signal of $-CH_2$ deformation indicates a higher degree of cross-linking and mono-/oligomer conversion and is expected to indicate a higher cytocompatibility. For these resins, no difference between the extraction media is distinguished, but the degree of crosslinking increases with increasing UV exposure times (Fig. 4E and F).

The Raman peaks of the photo sensitizer and the photo initiator are not visible in the spectra of the mixtures because of their low concentration (Fig. 4B and C). In the beginning of the measurements, a high amount of fluorescence was identified in the Raman spectra, which diminished with UV exposure time (Fig. S2, ESI†). The effect of this fluorescence and changes in peak ratios on transparency and cytocompatibility were observed in the experiments with UV/VIS spectrophotometry and in cell experiments as described later.

2.5. Cytocompatibility

UV exposure and solvent extraction with water or alcohol have been shown to improve cytocompatibility and cell proliferation.[11,14,24,42] We therefore conducted a study on how post-treatment variations influence biocompatibility with L929 mouse fibroblasts, and HUVECs as primary endothelial

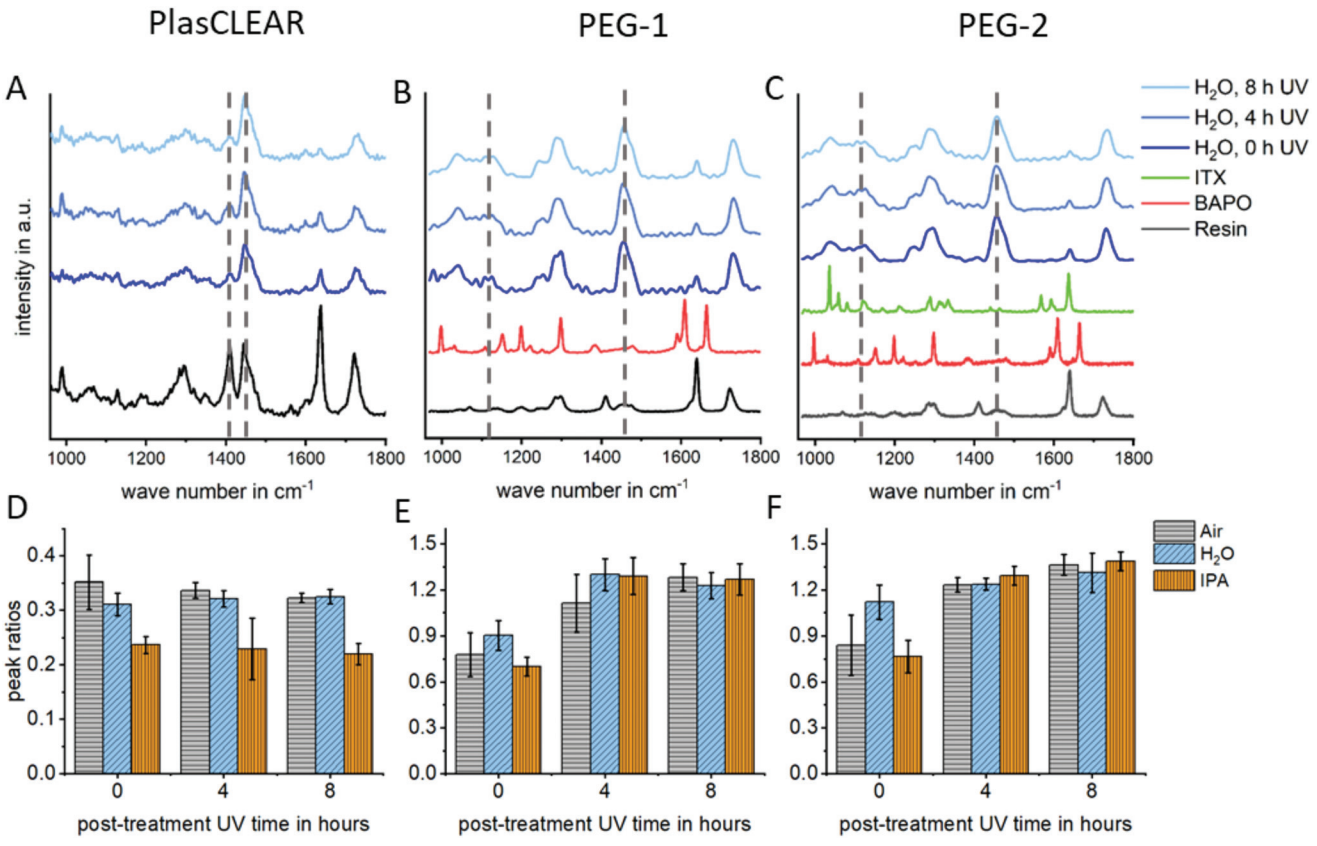

Fig. 4 Results of Raman spectroscopy on printed parts depending on the post-treatment. Fingerprint region spectra of PlasCLEAR resin (A), PEG-1 (B) and PEG-2 (C) with marked peaks used to calculate peak ratios. Peak ratios as degree of cross-linking are given for peaks at 1410 : 1470 cm^{-1} for PlasCLEAR (D) and at 1130 : 1470 cm^{-1} for PEG-1 (E) and PEG-2 (F).

cells. Resazurin conversion compared to the control group was measured with a CellTiter Blue assay after two days in contact with printed samples.

For PlasCLEAR, the resazurin conversion increased for L929 fibroblasts compared to the positive control with increased UV exposure time (Fig. 5A). Additionally, overnight extraction in IPA resulted in higher metabolic activity even at 0 h UV exposure time compared to water or air extraction, which was very dominant for HUVECs (Fig. 5B). This correlates to Raman spectroscopy data, which showed that IPA decreases the amount of reactive C=C bonds in printed parts compared to the extraction in water or air. However, cell cultivation in contact with printed parts was possible with HUVECs even after water extraction and 8 hours UV exposure (Fig. S4, ESI†).

As expected from Raman spectroscopy and UV/VIS spectrophotometry, the influence of the selected solvent medium (water, IPA or no medium) could not be observed for PEG-DA based resins. For both PEG-1 and PEG-2, cell viability increased with increasing UV exposure time independent of the solvent. This is in line with previous reports, where cytotoxic effects of the photo initiator were observed,[29] which could be countered by prolonged UV exposure.[11] In our case, an UV exposure time of 4 hours was enough for HUVECs to survive when cultured on printed parts, independent on solvent extraction (Fig. S5 and S6†). For both PlasCLEAR and PEG-2, lower metabolic activity for HUVECs compared to the control group was observed, but not for L929 fibroblasts. This could indicate a certain impact on cell viability of these parts, but cell culturing with no peculiar morphological changes was possible for up to a week.

2.6. Transparency of prints

Printed parts have to exhibit high transparency in the visible light range for bright-field as well as fluorescence microscopy and further spectrometric assays. While all three resins appear transparent to the eye (Fig. 2B), we conducted UV/VIS spectrophotometry on printed parts to quantify transparency and identify differences in transmission related to post-treatment procedures (Fig. 6A1–C1).

No trend regarding post-treatment could be distinguished for the commercial PlasCLEAR resin. This is in contrast to Raman spectroscopy results, which indicated a reduction of reactive C=C bonds with IPA extraction. However, UV/VIS spectrophotometry reveals that even with extensive post-treatment, no light is transmitted at wavelengths below 400 nm (Fig. 6, Fig. S3, ESI†). This indicates that certain components of the resin, which absorb all light below 400 nm, remain inside the prints (Fig. 2A). These transmission properties

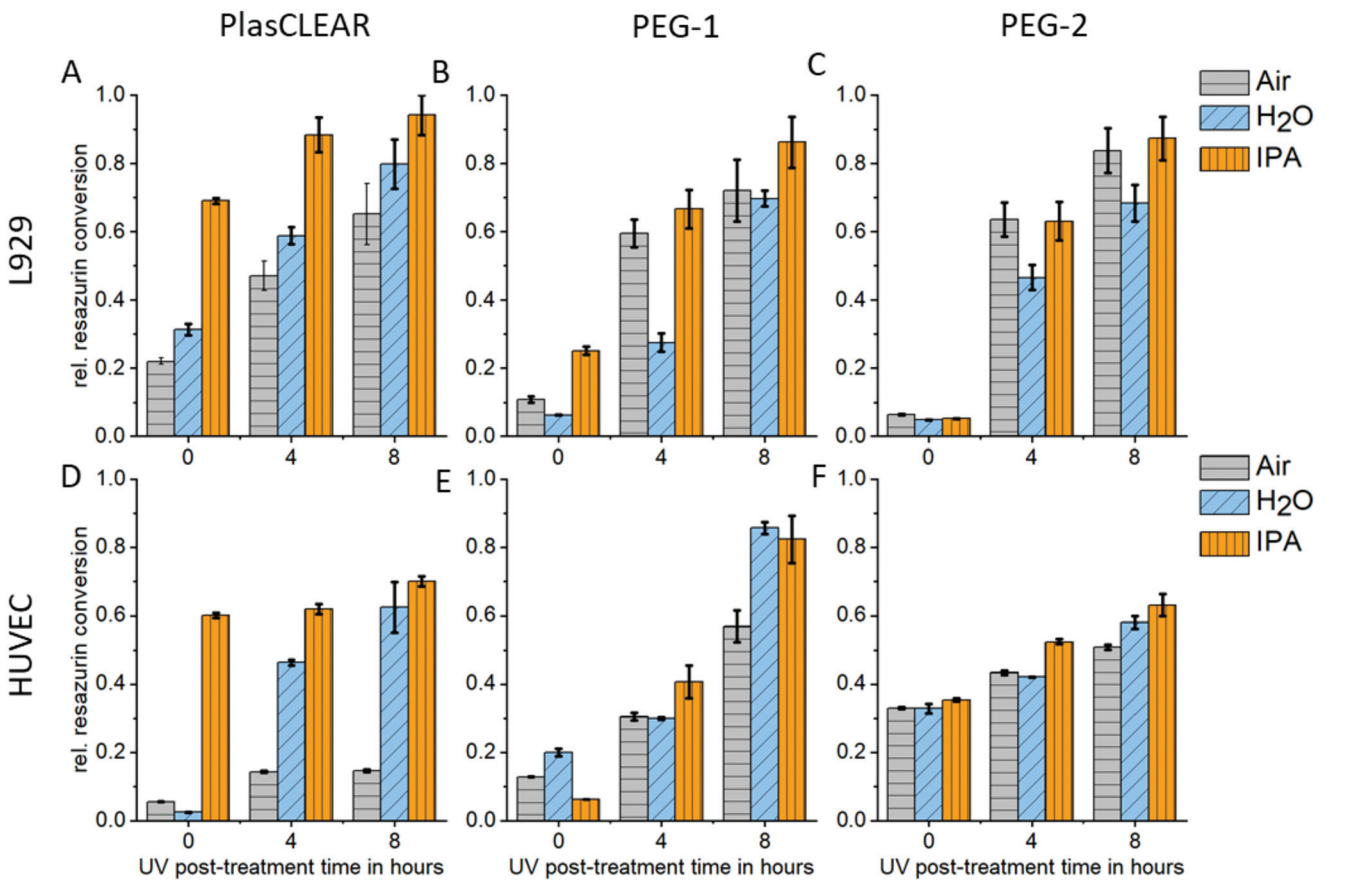

Fig. 5 Relative resazurin conversion rate compared to control group for L929 (A–C) and HUVECs (D–F) cells cultivated near PlasCLEAR (A and D), PEG-1 (B and E) and PEG-2 (C and F) printed parts in dependence on post-treatment extraction medium and UV exposure time.

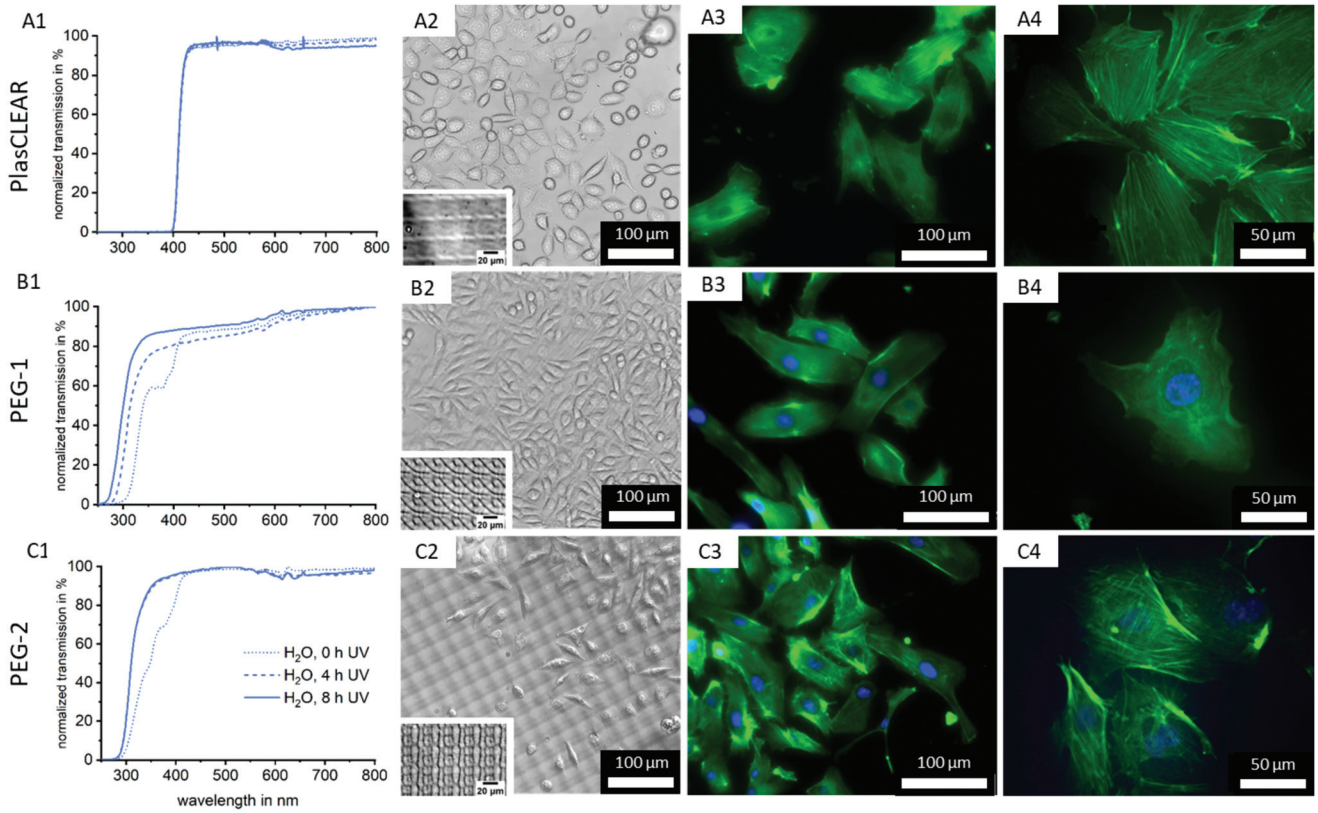

Fig. 6 Normalized transmission spectra obtained by UV/VIS spectrophotometry of PlasCLEAR (A1), PEG-1 (B1) and PEG-2 (C1) printed parts with water extraction and UV exposure times of 0 h, 4 h, and 8 h. Microscopy images were obtained of cells cultured on printed parts after post-treatment. Phase contrast images show L929 mouse fibroblasts for all three resins (A2, B2 and C2). A periodic pattern is visible in these images, which is shown enlarged as an inset in the images and is caused by the mirrors of the DLP. Fluorescence microscopy images of HUVECs stained with DAPI (blue) for cell nuclei and Alexa Fluor 488-phalloidin (green) for actin filaments at (A3, B3 and C3) 200× and (A4, B4 and C4) 400× magnification.

make PlasCLEAR resin suitable for general light microscopy but not for fluorescent microscopy with certain dyes. Staining of cell nuclei with DAPI, which has an excitation wavelength of 360 nm, is not possible when the excitation occurs through the prints like in inverse microscopes. This limits the possible application of PlasCLEAR for advanced light microscopy. To overcome this limitation, alternative dyes or upright, reflected light microscopy instead of inverse, transmitted light microscopy can be employed. However, this change of microscope is not possible in the case of microfluidic chips for OOC.

In contrast, both PEG-DA based resins transmit light at wavelengths above 300 nm and are therefore suitable in combination with the most commonly applied fluorescent dyes (Fig. 6B1 and C1). For PEG-1, two significant changes occur with increasing UV exposure time. With 4 hours of UV exposure, the dent in the transmission at 360–380 nm vanishes with the removal of photo initiator residues (compare to Fig. 2A). Additionally, with increased UV exposure time, the transmission edge is shifted to lower wavelengths, which is more dominant at 8 hours UV exposure than for 4 hours (Fig. 6B1 and C1).

The same effect on the transmission properties after 4 hours UV exposure can be seen for PEG-2. In this case, the two dents in the transmission can be correlated to the photo initiator as for PEG-1, and to the photo sensitizer (370–390 nm). A shift of the transmission edge also occurs, but not as strong as for PEG-1. In summary, a clear improvement of transmission with increasing UV exposure time can be observed, without significant influence of the extraction medium type for both PEG-DA based resins (Fig. S3, ESI†). This is in line with Raman results, where UV exposure time can be correlated to an increase in polymer cross-linking and conversion rate.

2.7. Cell culture on printed parts

As a next step, we cultivated both L929 (Fig. S7, ESI†) and HUVECs on the printed parts to test the suitability of transparent printed culture dishes for light microscopy and fluorescence imaging of cells (Fig. 6A2–C4). This was possible after plasma activation of the surface, which facilitates wetting and cell adhesion as shown by contact angle measurements (Fig. 3C).

Phase contrast imaging as well as fluorescence microscopy was successful for all three materials, and detailed cell images could be acquired at high magnifications (Fig. 6). This confirms the high quality of the 3D-printed cell culture dishes

regarding optical properties as well as cell attachment. It also proves that 3D-DLP-printing is an exciting, high-quality alternative to standard lab ware or soft lithography.

As expected from UV/VIS measurements, the cell nuclei stained with DAPI cannot be detected when cells are cultured on printed PlasCLEAR Petri dishes. However, actin filaments stained in green are clearly visible, and 400-times magnification images are of high quality. For any cell culture application that does not require blue fluorescence dyes, PlasCLEAR remains a good material offering high biocompatibility and great microscopy properties. Both PEG-DA based materials offer the same quality for phase contrast and fluorescence microscopy, but exhibit the clear advantage of visible DAPI staining, as these materials are fully transparent in this spectrum. For PEG-2, a periodic pattern becomes dominant in the phase contrast image, which slightly disturbs bright-field imaging. This periodic pattern is visible for all three materials under the light microscope when no cells are cultured (Fig. 6A2, B2 and C2 insets). The cause for this are the printer's DLP pixel, which reproduce surface features in the printed parts as shown by AFM measurements (Fig. S8, ESI†). The periodic height variations only cover 40 nm for PlasCLEAR and PEG-1, hence they are not visible when cells are covering the prints' surface. The photo sensitizer amplifies this pattern to 400 nm in PEG-2, which therefore becomes dominantly visible under the microscope. Fortunately, this pattern is not observed in fluorescence microscopy and does not influence the output even at high magnifications. Additionally, this pattern could possibly be actively employed to direct cell alignment and direction,[43,44] as the height of imprinted pixels can be tailored by the amount of ITX.

In summary, PEG-1 offers the best properties for monitoring cells under the microscope, but both other materials are also suitable with slight limitations.

2.8. Application as OOC – printing resolution

The previous experiments showed that DLP-printing of commercial or self-mixed acrylate-based resins is a suitable method to produce highly transparent and cytocompatible parts that support cell growth and enable high-resolution microscopy. These are fundamental requirements when DLP-printing is used for specialized lab ware and microfluidic systems for OOC. As a next step, the resolution of the printer in combination with the resins has to be quantified and optimized. We therefore printed pillars and holes with both round and square layouts, which are of interest for cell biological applications (Fig. 7J and K). We then analyzed their shape fidelity with CLSM and light microscopy (Fig. 7A–I). A design of experiments was conducted to identify the parameters that most influence the print resolution. In accordance with our expectation, the results indicated that light intensity and exposure time at a certain slice thickness, thus the total energy input per volume, are the dominant factors[13,21] (Fig. S9, ESI†). For positive features such as pillars, a higher energy input is favorable, while a lower energy input improves the quality of negative features like holes and channels. This could lead to a trade-off situation in some cases, and the final print parameters have to be adapted to the specific application, possibly taking into account that the maximum resolution cannot be achieved if both positive and negative features are to be combined.

The study also revealed that freestanding pillars of only 50 µm (only two DLP pixels) in diameter and 250 µm in height can be achieved with all three resins (Fig. 7A–C). This resolution is high enough for most OOC applications, which often require channels separated from gel chambers by small pillars. These small pillars can also be used to guide the generation of vascular structures.[3] When printed as 500 µm long and

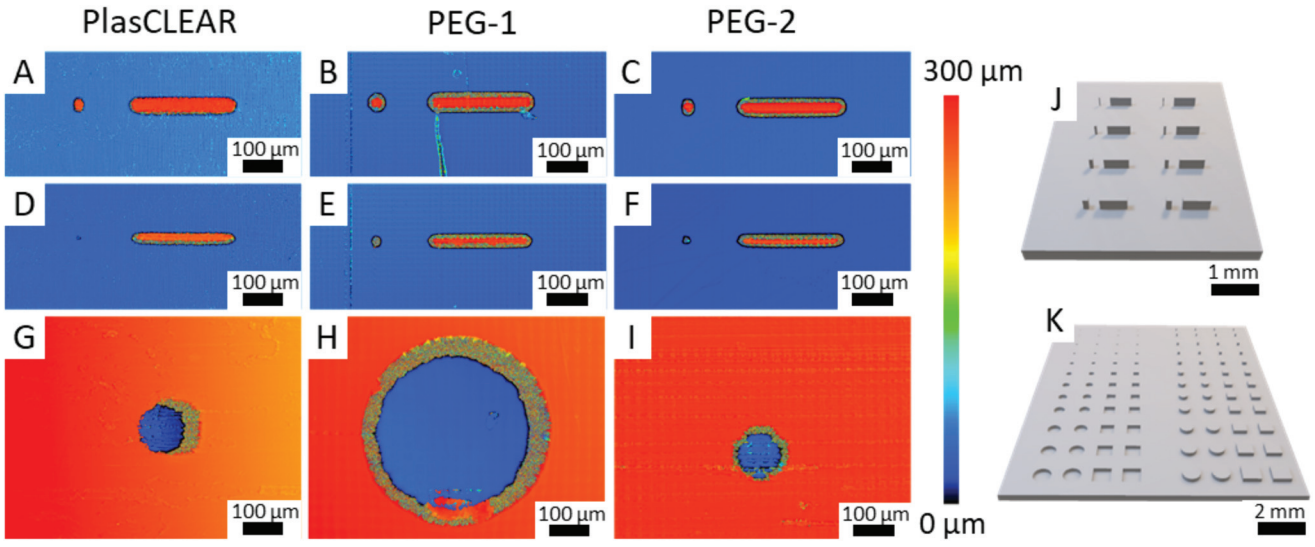

Fig. 7 CLSM height images of printed pillars, walls (A–F) and holes (G–I). With all three resin, a minimum pillar size of 50 µm (A–C), and minimum wall size of 35 µm (D and E) could be printed. Minimum hole size varies with resin, and is 120 µm for PlasCLEAR (G), 370 µm for PEG-1 (H) and 100 µm for PEG-2 (I). CAD models for testing the maximum resolution for freestanding pillars and walls (J) and holes (K).

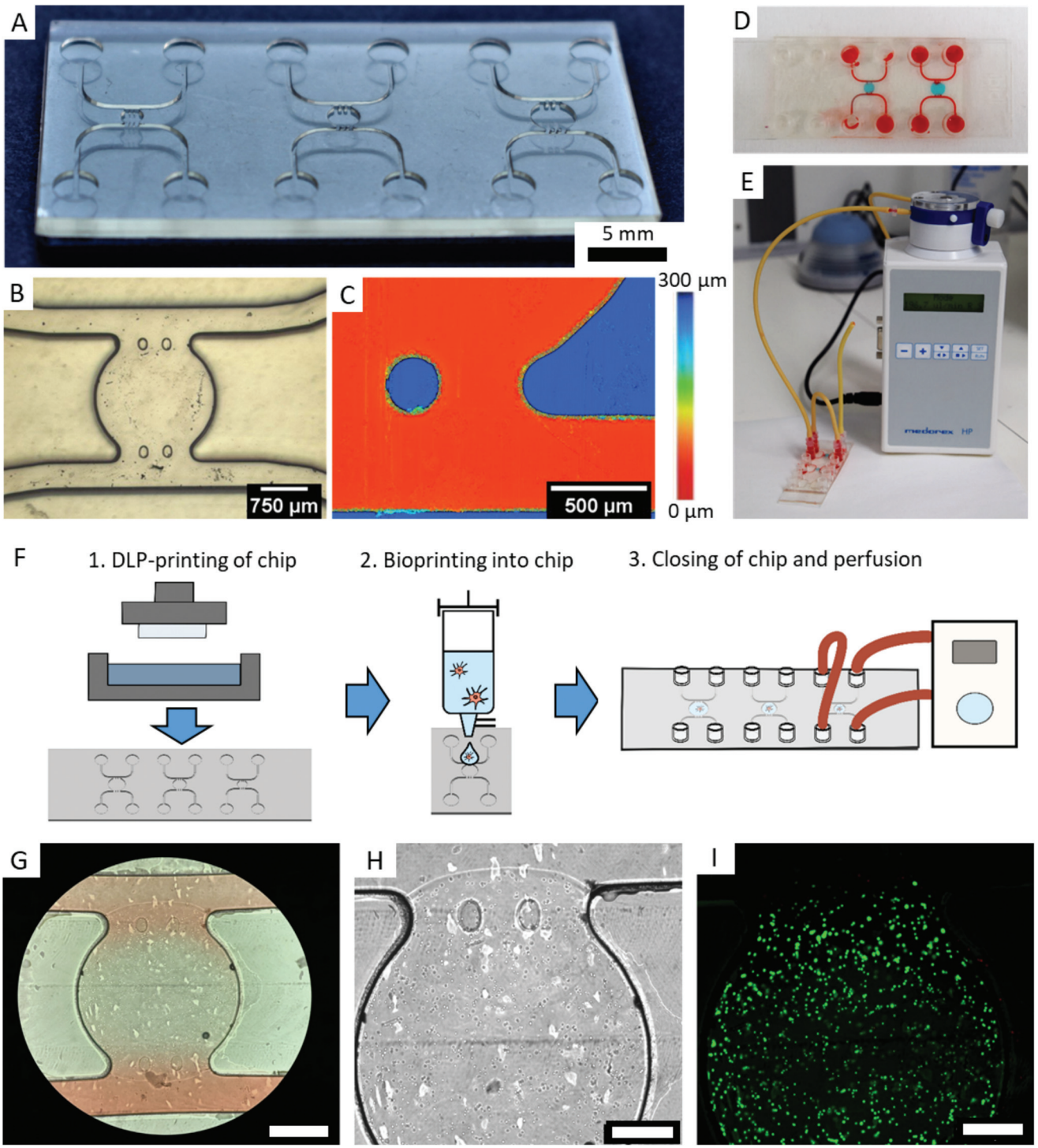

Fig. 8 DLP-printed microfluidic chip for OOC application with a main chamber, separated from two channels by two round pillars (A). The printed chip has a chamber diameter of 2 mm, a channel width of 500 µm, a pillar diameter of 250 µm and a height of 250 µm (B). CLSM image shows the correctly printed height and the clear edges (C). To obtain an OOC, the chamber can be filled with a hydrogel (blue), closed with a lid and perfused with liquid (red) *via* the Luer ports (D), which also enable the connection to a perfusion system (E). A schematic representation of the fabrication process shows the DLP printing of the chip, followed by the microvalve drop based bioprinting of a cell-containing hydrogel. The chip is closed with a lid and connected to a perfusion system (F). As a model OOC, L929 mouse fibroblasts were bioprinted into the microfluidic chip's chamber. Light microscopy shows how the cell culture medium flows through the channel, but not into the agarose gel in the cell (G). Cells are encapsulated in the gel in the main chamber (H) and remain viable under perfusion for two days as shown by live/dead staining (I). Scale bar showing 1000 µm (G) and 500 µm (H, I).

Table 1 Summary of properties of resins regarding their suitability for OOC fabrication. Qualitative rating of material properties given with + + (very good), + (good), o (neutral), – (poor) and – – (very poor)

Property	PlasCLEAR	PEG-1	PEG-2
Transparency (vis range)	o $\lambda > 400$ nm	+ +	+ +
Microscopy	o No DAPI	+ +	o Pixel structure visible in phase contrast imaging
Biocompatibility	+	+ +	o
Print resolution	+ 50 μm pillars 120 μm holes	o 50 μm pillars 370 μm holes	+ + 50 μm pillars 100 μm holes
Printing time	– –	+	+ +
Surface waviness	+ + 40 nm	+ + 40 nm	– – Over 400 nm
Post-treatment steps	IPA extraction, 4 hours UV exposure	8 hours UV exposure	8 hours UV exposure

250 μm high walls, the minimum feature width could further be reduced to only 35 μm, which is only slightly more than a single DLP pixel (Fig. 8D–F). While all materials proved to be great for producing positive features, overcuring is a more dominant challenge for negative features (holes and channels). In this regard, clear differences between the applied resins can be observed. PEG-1 offers the worst performance with a minimum hole diameter of 370 μm (Fig. 7H). This could greatly be improved by adding a very small amount of photo sensitizer (0.1 wt/vol%) in PEG-2, which reliably produces holes with a diameter of only 100 μm (four DLP pixels, Fig. 7I). The photosensitizer ITX has already been used in higher concentrations to increase the resolution before.[13] However, decreasing the amount of ITX is beneficial regarding optical and cytotoxic properties of the printed parts[18] (Fig. 5 and 6). Finally, PlasCLEAR could not match the before mentioned resolutions, but still offers good printing properties and acceptable feature sizes, resulting in holes of 120 μm diameter (Fig. 7G).

Comparing the three materials, PEG-1 is best suited to print general cell culture equipment that does not require small holes or channels, as it offers superior transparency, microscopy characteristics and high cytocompatibility. PEG-2 and PlasCLEAR are suitable for more complex geometries and microfluidics for OOCs. Applications of PlasCLEAR are limited regarding immunofluorescence assays, but the material exhibits good cytocompatibility and is a suitable candidate for bright-field microscopy. Of all materials, PEG-2 offers the best print resolution for negative features and potentially for closed channel systems, whereas its surface topography artefacts might influence cell growth.

2.9. Application as OOC – microfluidic chip fabrication

We designed a microfluidic chip to test the usability of transparent DLP-printing for OOCs by applying the previously found printing parameters. The design is similar to typical PDMS casts, with straight walls and an open top (Fig. 8A). This design has the advantage that it can be combined with any available bioprinting technology to create complex cellular architectures inside. Additionally, the challenge in 3D-printing closed and still highly transparent channels is avoided, and no residual resin can impede the laminar flow inside the channel. The microfluidic chip contains a central chamber of 2 mm diameter, which constitutes the future organoid compartment of the device. It is supplied with culture medium *via* two independent fluidic channels, from which it is separated by two pillars, which prevent gel from penetrating into the channels (Fig. 8B). A further advantage of 3D-printing over soft-lithography becomes prominent in the height image of the microfluidic chip, which measures 250 μm in height (Fig. 8C). In DLP-printing, chip heights between 50 and 1000 μm can simply be printed in a short time, while heights over 100 μm are difficult and time consuming to achieve with SU-8 spin coating and soft lithography processes. In particular, the microfluidic chip with negative features of 250 μm depth (Fig. 8C) would be challenging to produce using soft lithography. The central chamber can be filled with a cell-containing hydrogel manually or, as shown in this work, with a microvalve based DoD bioprinter with agarose and fibroblasts (Fig. 8D). The device is sealed after printing with a lid containing the Luer connectors and connected to a perfusion system (Fig. 8E and F).

Microscopy images show that the bioprinted agarose gel containing mouse fibroblasts remains stable in the central chamber for various days. The fibroblasts exhibited a high cell viability on day two (Fig. 8G–I). The chip did not leak under shear rates of 10 dyn cm^{-2} after two days, and fluorescence staining inside the chip was successfully performed with a standard staining protocol as used with PDMS chips.

3. Conclusion

Additive manufacturing, especially DLP-printing, appears as a promising alternative to *e.g.* soft lithography and PDMS molding for specially tailored lab ware and microfluidic systems. To become competitive, DLP-printed devices have to exhibit superior optical properties such as transparency, high post-printing biocompatibility and highly resolved features.

In this work, we could show that the commercial PlasCLEAR resin and the PEG-DA based mixtures are suitable for the fabrication of transparent, cytocompatible and finely

structured microfluidic chips. To achieve this, first of all modification of the printer hardware was shown to be essential in order to achieve an even surface and reduce roughness as well as bulk defects. The three acrylate-based materials offer mechanical properties and a wetting behavior closely matching polystyrene, allowing to simply replace standard lab ware by printed parts. In addition, the absorbance of small hydrophobic molecules and of bovine serum albumin is two to three orders of magnitude smaller than for PDMS, demonstrating the advantage of these materials for quantified culture assays or pharmacokinetics. Post-treatment steps as UV exposure and solvent extraction were critical to improve light transmission and to achieve biocompatibility, which we tested for the L929 fibroblast cell line and for primary HUVECs. Cell culture on printed parts was successful for all three resins, with prints exhibiting good microscopy properties even at high magnification fluorescence microscopy. We were able to print very fine structures like freestanding, high aspect ratio pillars with a minimum diameter of only 50 μm (two DLP pixels) and walls with a width of 35 μm with all three resins, exhibiting the excellent resolution of DLP-printing.

Our study revealed strong differences between the employed materials, in particular with respect to their optical properties, the required post-treatment steps, their cytocompatibility as well as the achievable print resolution (Table 1). The results indicate that both the selected material and the associated printing parameters must be carefully chosen and adapted to the desired application. However, biocompatibility, general transparency and a print resolution of 50 μm is achieved by all three materials.

By translating these findings into a stable 3D-printing process, we were able to fabricate a 3D-bioprinting compatible microfluidic chip. We successfully filled this chip with a cell-containing hydrogel using a microvalve-based bioprinter and cultured this basic OOC-model for two days under perfusion. This model OOC showed no leakage during dynamic cultivation. Microscopy and staining protocols could be employed using previously established methods and protocols without noticeable difference to so far applied PDMS chips.

The results prove that transparent DLP-printing can greatly impact research on cell culture in 2D and 3D by replacing standard lab ware, usually made of PS or produced by soft lithography and PDMS molding. Modification of the printer hardware and careful post-treatment routines are the most important features that enable successful cell culture applications. In future, we expect further developments regarding resin compositions that are specifically tailored to certain application cases, commercially available print systems for transparent printing and research on functionalized resins (*e.g.* for cell guidance, wetting behavior, bioactuators). Ultimately, with appropriate further development, we see enormous potential for the future fusion of different additive manufacturing processes, such as SL printing and 3D bioprinting, for the production of biophilic multifunctional materials and complex OOC systems.

4. Experimental

4.1. Resin composition

Three resin compositions were used. The commercial resin PlasCLEAR (Litholabs/Asiga, Heidelberg, Germany) was directly printed. The resins PEG-1 and PEG-2 were first formulated and then printed. As PEG-1 we refer to poly(ethylene glycol) diacrylate (PEG-DA) M_w 200 (Merck KGaA, Darmstadt, Germany) mixed with 0.4 wt/vol% phenylbis(2,4,6-trimethylbenzoyl)phosphine oxide (BAPO) (Merck KGaA, Darmstadt, Germany) as photo initiator. PEG-2 is a mixture of PEG-DA with 0.4 wt/vol% BAPO as photo initiator and 0.1 wt/vol% 2-isopropylthioxanthone (ITX) (abcr GmbH, Karlsruhe, Germany) as photo sensitizer. The PEG-DA based resins were prepared by adding the powder photo initiator and sensitizer to the liquid PEG-DA, followed by stirring with a magnetic stir bar on a heating plate at 40 °C for one hour.

4.2. 3D-DLP-printing

For 3D-printing, an Asiga Pico 2^{HD} 27 stereolithography printer (Litholabs/Asiga, Heidelberg, Germany) with a print volume of (54.43 × 30.54 × 70.00) mm^3 was used. The printing and post-treatment steps were conducted in a UV-radiation protection cleanroom environment to prevent the resins from uncontrolled curing.

For experiments testing the maximum resolution of the printer, the printer was used as delivered by the manufacturer. To achieve transparency, the manufacturer's vat was replaced by a borosilicate glass Petri dish (Carl Roth GmbH + Co. KG, Karlsruhe, Germany) with a diameter of 12 cm and a bottom thickness of 2 mm. The Petri dish was cleaned with ethanol and then coated with a siliconizing reagent named Sigmacote (Merck KGaA, Darmstadt, Germany). Before use, the Petri dish was rinsed with water to remove excess Sigmacote and reaction products. The glass vat was then attached to the bottom of the printer with adhesive tape (tesa SE, Norderstedt, Germany). The printer's build plate was also replaced by a custom-built plate made of highly polished and hardened 42CrMo4 steel. STL-files of print geometries were created in AutoCAD 2018 (Autodesk, San Rafael, USA).

Print parameters were varied for each resin and adapted to the specific target structure, with higher energy inputs for maximum resolution of pillars and lower energy input for holes and channels. The slice thickness was set between 10 and 25 μm. Light intensity varied between 10 and 20 mW cm^{-2} for PlasCLEAR and PEG-1, and 5–20 mW cm^{-2} for PEG-2. The exposure time for PlasCLEAR was 10–30 s, 0.5–0.8 s for PEG-1, and 0.2–0.8 s for PEG-2.

4.3. Post-processing

After printing, the samples were washed with isopropanol and then treated for 10 minutes in isopropanol in an ultrasonic bath. The washing step was followed by a post-curing step in water for 10 minutes under the Asiga Flash UV chamber (Litholabs/Asiga, Heidelberg, Germany). For further

post-treatment steps, samples were then left in water, isopropanol or on air overnight and post-cured for additional 0, 4 or 8 hours.

4.4. Optical analysis

Printed parts were analyzed with the bright field and fluorescence microscope Leica DM4000M (Leica, Wetzlar, Germany) as well as with the VK-8700 Color 3D CLSM (Keyence Corporation, Osaka, Japan) with a laser wavelength of 658 nm.

4.5. Roughness measurements

For images and area scans of the surface roughness a VK-8700 Color 3D CLSM (Keyence Corporation, Osaka, Japan) with a laser wavelength of 658 nm was used. Quantification of roughness parameters was done with DektakXT profilometer (Bruker Corporation, Billerica, USA) according to EN ISO 25178 with a tip radius of 2.5 μm.

4.6. Mechanical characterization

To determine the elastic modulus, a Nano Indenter G200 (Keysight Technologies Inc., Santa Rosa, USA) with a Berkovich tip was used. The indentation depth was set to 5000 nm and the tip oscillated at 45 Hz with a displacement of 2 nm during measurements. To calculate the elastic modulus, a Poisson ratio of ν = 0.375 was chosen for resins and PS, and ν = 0.475 for PDMS. For each material, 16 indents were averaged.

4.7. Contact angle measurements

Wetting behavior was analyzed with a contact angle goniometer drop shape analyzer DSA 100 (Krüss GmbH, Hamburg, Germany). 1.5 μl droplets of deionized water were pipetted onto printed parts with and without plasma treatment. For comparison, measurements were also done on a slab of native PDMS (Sylgard-184, Dow Corning Inc., Midland, USA), a glass microscopy slide and polystyrene Petri dish (Greiner AG, Kremsmünster, Austria) with n = 8. For plasma treated samples, samples were placed in a plasma chamber (Nano, Diener Electronic, Ebhausen, Germany) under oxygen atmosphere for 1 minute at 75% power. The contact angle was automatically calculated.

4.8. Diffusivity

Rectangular wells with a side length of 2 mm and height of 1 mm were printed with all three materials and post-treated. For PDMS, a negative mold was printed and PDMS cured at a ratio of 10 : 1. Nile Red was dissolved in DMSO at a concentration of 1 μg ml^{-1}, while FITC-BSA (all from Merck KGaA, Darmstadt, Germany) was diluted in PBS to a concentration of 50 μg ml^{-1}. The wells were filled with the dye for 30 min for Nile Red and 15 min for FITC-BSA, then washed two times with water. The fluorescence intensity was measured with a microscope. Two intensity profiles for three samples were taken using ImageJ and the diffusion coefficient was determined by fitting the fluorescence intensity profile using Fick's 2nd law of diffusion.

4.9. Raman spectroscopy

For Raman measurements, an alpha 300R confocal Raman microscope (WITec GmbH, Ulm, Germany) with a second harmonic Nd:YAG laser at 532 nm wavelength and a 10×/0.25 objective was used. For measurements of printed parts and resins, the laser intensity was set to 3 mW and 10 accumulations were taken at 0.5 s integration time each. Raman spectra were flattened using a FFT-flattening function and peak ratios calculated by integrating over the peak area. Integration ranges were set as 1010 to 1160 (C–C stretching vibrations, various C–O–C bond modes), 1380 to 1420 (C=C stretch) and 1420 to 1520 cm^{-1} (–CH_2 deformation mode).

4.10. UV/VIS measurements

UV/VIS spectrophotometry was done on the resins as well as on their individual components diluted in dichlormethane (Merck KGaA, Darmstadt, Germany) using a V-630 spectrophotometer (Jasco Deutschland GmbH, Pfungstadt, Germany). The printer's LED spectrum was recorded with an AvaSpec-3648 spectrophotometer (Avantes, Apeldoorn, Netherlands). The same spectrophotometer was used in combination with an Avalight-DH-S-BAL halogen light source (Avantes, Apeldoorn, Netherlands) for measurements of printed parts depending on post-processing. For each spectrum, 100 measurements with an integration time of 600 μs were averaged.

4.11. AFM measurements

For detailed surface inspection, a Dimension Icon AFM (Bruker Corporation, Billerica, USA) with a RTESPA-300 cantilever with a spring constant of 40 N m^{-1} and resonance frequency of 30 kHz (Bruker Corporation, Billerica, USA) in PeakForce tapping mode was used. Images were processed with a first order plane fit followed by a median of differences line fit.

4.12. Cell culture

For cell experiments, L929 mouse fibroblasts (Sigma-Aldrich, St Louis, USA) at passage 15 and HUVECs (PromoCell GmbH, Heidelberg, Germany) at passage 3 were used. Cells were cultured in DMEM (Thermo Fisher Scientific Inc., Waltham, USA) supplemented with 10% FBS (Thermo Fisher Scientific Inc., Waltham, USA) and 1% PenStrep (Thermo Fisher Scientific Inc., Waltham, USA) and Endothelial Growth Medium Kit (PromoCell GmbH, Heidelberg, Germany), respectively.

For the biocompatibility study, cells were seeded in a 96 well plate (VWR International, Radnor, USA) at 15 000 cells per cm^2. 24 hours later, cells were washed and new medium added along with post-processed prints (cylinders with 3 mm in height and diameter); and control groups cultivated as well. After another 48 hours, a CellTiter Blue assay (Promega Corporation, Fitchburg, USA) was performed and conversion measured with an Infinite M Plex plate reader (Tecan Group AG, Männedorf, Switzerland). Relative resazurin conversion was calculated by subtraction of the medium-only well signal and normalized to the positive control average signal.

For cell cultivation on printed parts, small Petri dishes (10 mm inner diameter) were printed and post-processed as described. Before cell seeding, the printed parts were plasma treated in a plasma chamber (Nano, Diener Electronic, Ebhausen, Germany) under oxygen atmosphere for 1 minute at 75% power. Immediately, cells were seeded on top of the treated surface at a density of 10 000 cells per cm^2. Medium was changed once on day 2 and images were taken at day 4. Bright field, phase contrast and fluorescence microscopy were conducted on a light microscope (Echo Revolve, Discover Echo Inc., San Diego, USA). For immunofluorescence staining, cells were fixed in 4% paraformaldehyde (Carl Roth GmbH + Co. KG, Karlsruhe, Germany) for 10 minutes and permeabilized with 0.5% Triton X-100 in PBS (Carl Roth GmbH + Co. KG, Karlsruhe, Germany) for 5 minutes. Actin filaments were stained for 30 minutes with Alexa Fluor 488 Phalloidin (Thermo Fisher Scientific Inc., Waltham, USA) and for 3 minutes with DAPI (Sigma Aldrich, St Louis, USA).

4.13. OOC experiments

For the OOC, a microfluidic chip of 250 μm height with 500 μm wide channels, a 2 mm diameter central chamber and 250 μm diameter pillars was printed with PlasCLEAR resin. The chip was post-treated with an isopropanol extraction and 8 hours of UV exposure. A 1 wt/vol% agarose gel (Sigma-Aldrich, St Louis, USA) was mixed with L929 cells with a final concentration of 10^6 cells per ml and printed into the chip with a drop-on-demand 3D-bioprinter (SuperFill-Robo, Black Drop Bioprinter GmbH, Aachen, Germany). The chip was sealed with a custom-made Luer top slide (ibidi GmbH, Gräfelfing, Germany) and connected to a peristaltic pump (Medorex HP, Nörten, Germany). The chip was perfused for two days, after which live/dead staining was performed with propidium iodide (Carl Roth GmbH + Co. KG, Karlsruhe, Germany) and fluorescein diacetate (Sigma Aldrich, St Louis, USA) prior to imaging.

Conflicts of interest

There are no conflicts to declare.

Acknowledgements

The authors thank the Deutsche Forschungsgemeinschaft (Project ID 265191195 – SFB 1194, Project A07 and Sachbeihilfe DI 2176/2-1) for financial support. In addition, we thank Dominik Herold and Jonas Kind from the group of Prof. Christina M. Thiele (Clemens-Schöpf-Institute for Organic Chemistry and Biochemistry, Technical University of Darmstadt) for their support with UV/VIS measurements, Christian Dietz (Physics of Surfaces, Technical University of Darmstadt) for AFM measurements and Sebastian Bruns (Department of Physical Metallurgy, Technical University of Darmstadt) for support with nanoindentation experiments.

References

1 D. Caballero, S. M. Blackburn, M. De Pablo, J. Samitier and L. Albertazzi, Tumour-vessel-on-a-chip models for drug delivery, *Lab Chip*, 2017, **17**, 3760–3771.
2 M. Carve and D. Wlodkowic, 3D-printed chips: Compatibility of additive manufacturing photopolymeric substrata with biological applications, *Micromachines*, 2018, **9**, 91.
3 A. Fritschen and A. Blaeser, Biosynthetic, biomimetic, and self-assembled vascularized Organ-on-a-Chip systems, *Biomaterials*, 2020, **268**, 120556.
4 S. N. Bhatia and D. E. Ingber, Microfluidic organs-on-chips, *Nat. Biotechnol.*, 2014, **32**, 760–772.
5 S. Halldorsson, E. Lucumi, R. Gómez-Sjöberg and R. M. T. Fleming, Advantages and challenges of microfluidic cell culture in polydimethylsiloxane devices, *Biosens. Bioelectron.*, 2015, **63**, 218–231.
6 A. M. Ghaemmaghami, M. J. Hancock, H. Harrington, H. Kaji and A. Khademhosseini, Biomimetic tissues on a chip for drug discovery, *Drug Discovery Today*, 2012, **17**, 173–181.
7 L. Ewart, E.-M. Dehne, K. Fabre, S. Gibbs, J. Hickman, E. Hornberg, *et al.*, Application of Microphysiological Systems to Enhance Safety Assessment in Drug Discovery, *Annu. Rev. Pharmacol. Toxicol.*, 2018, **58**, 65–82.
8 B. C. Gross, J. L. Erkal, S. Y. Lockwood, C. Chen and D. M. Spence, Evaluation of 3D printing and its potential impact on biotechnology and the chemical sciences, *Anal. Chem.*, 2014, **86**, 3240–3253.
9 A. K. Au, W. Huynh, L. F. Horowitz and A. Folch, 3D-Printed Microfluidics, *Angew. Chem.,– Int. Ed.*, 2016, **55**, 3862–3881.
10 C. M. B. Ho, S. H. Ng, K. H. H. Li and Y. J. Yoon, 3D printed microfluidics for biological applications, *Lab Chip*, 2015, **15**, 3627–3637.
11 A. Urrios, C. Parra-Cabrera, N. Bhattacharjee, A. M. Gonzalez-Suarez, L. G. Rigat-Brugarolas, U. Nallapatti, *et al.*, 3D-printing of transparent bio-microfluidic devices in PEG-DA, *Lab Chip*, 2016, **16**, 2287–2294.
12 B. Grigoryan, S. J. Paulsen, D. C. Corbett, D. W. Sazer, C. L. Fortin, A. J. Zaita, *et al.*, Multivascular networks and functional intravascular topologies within biocompatible hydrogels, *Science*, 2019, **364**, 458–464.
13 A. P. Kuo, N. Bhattacharjee, Y. S. Lee, K. Castro, Y. T. Kim and A. Folch, High-Precision Stereolithography of Biomicrofluidic Devices, *Adv. Mater. Technol.*, 2019, **4**, 1–11.
14 C. Warr, J. C. Valdoz, B. P. Bickham, C. J. Knight, N. A. Franks, N. Chartrand, *et al.*, Biocompatible PEGDA Resin for 3D Printing, *ACS Appl. Bio Mater.*, 2020, **3**, 2239–2244.
15 H. Gong, B. P. Bickham, A. T. Woolley and G. P. Nordin, Custom 3D printer and resin for 18 μm × 20 μm microfluidic flow channels, *Lab Chip*, 2017, **17**, 2899–2909.
16 Y. T. Kim, J. S. Choi, E. Choi and H. Shin, Additive manufacturing of a 3D vascular chip based on cytocompatible hydrogel, *Eur. Polym. J.*, 2021, **151**, 110451.

17 H. K. Park, M. Shin, B. Kim, J. W. Park and H. Lee, A visible light-curable yet visible wavelength-transparent resin for stereolithography 3D printing, *NPG Asia Mater.*, 2018, **10**, 82–89.
18 N. Bhattacharjee, C. Parra-Cabrera, Y. T. Kim, A. P. Kuo and A. Folch, Desktop-Stereolithography 3D-Printing of a Poly (dimethylsiloxane)-Based Material with Sylgard-184 Properties, *Adv. Mater.*, 2018, **30**, 1800001.
19 I. Matai, G. Kaur, A. Seyedsalehi, A. McClinton and C. T. Laurencin, Progress in 3D bioprinting technology for tissue/organ regenerative engineering, *Biomaterials*, 2020, **226**, 119536.
20 F. Zhu, J. Skommer, N. P. MacDonald, T. Friedrich, J. Kaslin and D. Wlodkowic, Three-dimensional printed millifluidic devices for zebrafish embryo tests, *Biomicrofluidics*, 2015, **9**, 046502.
21 H. Gong, M. Beauchamp, S. Perry, A. T. Woolley and G. P. Nordin, Optical approach to resin formulation for 3D printed microfluidics, *RSC Adv.*, 2015, **5**, 106621–106632.
22 A. L. Beckwith, J. T. Borenstein and L. F. Velasquez-Garcia, Monolithic, 3D-Printed microfluidic platform for recapitulation of dynamic tumor microenvironments, *J. Microelectromech. Syst.*, 2018, **27**, 1009–1022.
23 S. Waheed, J. M. Cabot, N. P. Macdonald, T. Lewis, R. M. Guijt, B. Paull, *et al.*, 3D printed microfluidic devices: Enablers and barriers, *Lab Chip*, 2016, **16**, 1993–2013.
24 S. M. Oskui, G. Diamante, C. Liao, W. Shi, J. Gan, D. Schlenk, *et al.*, Assessing and Reducing the Toxicity of 3D-Printed Parts, *Environ. Sci. Technol. Lett.*, 2016, **3**, 1–6.
25 V. Carvalho, I. Gonçalves, T. Lage, R. O. Rodrigues, G. Minas, S. F. C. F. Teixeira, *et al.*, 3D printing techniques and their applications to organ–on–a–chip platforms: A systematic review, *Sensors*, 2021, **21**, 3304.
26 A. Naderi, N. Bhattacharjee and A. Folch, Digital Manufacturing for Microfluidics, *Annu. Rev. Biomed. Eng.*, 2019, **21**, 325–364.
27 J. P. Fouassier, X. Allonas and D. Burget, Photopolymerization reactions under visible lights: Principle, mechanisms and examples of applications, *Prog. Org. Coat.*, 2003, **47**, 16–36.
28 N. Bhattacharjee, A. Urrios, S. Kang and A. Folch, The upcoming 3D-printing revolution in microfluidics, *Lab Chip*, 2016, **16**, 1720–1742.
29 R. Bail, A. Patel, H. Yang, C. M. Rogers, F. R. A. J. Rose, J. I. Segal, *et al.*, The effect of a type I photoinitiator on cure kinetics and cell toxicity in projection-microstereolithography, *Procedia CIRP*, 2013, **5**, 222–225.
30 ASIGA Materials Safety Data Sheet for PlasCLEAR v2. 2017.
31 S. Takenaga, B. Schneider, E. Erbay, M. Biselli, T. Schnitzler, M. J. Schöning, *et al.*, Fabrication of biocompatible lab-on-chip devices for biomedical applications by means of a 3D-printing process, *Phys. Status Solidi A*, 2015, **212**, 1347–1352.
32 C. I. Rogers, J. V. Pagaduan, G. P. Nordin and A. T. Woolley, Single-monomer formulation of polymerized polyethylene glycol diacrylate as a nonadsorptive material for microfluidics, *Anal. Chem.*, 2011, **83**, 6418–6425.
33 P. Kim, H. E. Jeong, A. Khademhosseini and K. Y. Suh, Fabrication of non-biofouling polyethylene glycol micro- and nanochannels by ultraviolet-assisted irreversible sealing, *Lab Chip*, 2006, **6**, 1432–1437.
34 G. González, D. Baruffaldi, C. Martinengo, A. Angelini, A. Chiappone, I. Roppolo, *et al.*, Materials testing for the development of biocompatible devices through vat-polymerization 3d printing, *Nanomaterials*, 2020, **10**, 1–13.
35 Y. T. Kim, S. Bohjanen, N. Bhattacharjee and A. Folch, Partitioning of hydrogels in 3D-printed microchannels, *Lab Chip*, 2019, **19**, 3086–3093.
36 M. Popal, J. Volk, G. Leyhausen and W. Geurtsen, Cytotoxic and genotoxic potential of the type I photoinitiators BAPO and TPO on human oral keratinocytes and V79 fibroblasts, *Dent. Mater.*, 2018, **34**, 1783–1796.
37 A. Skardal, D. Mack, A. Atala and S. Sokern, Substrate elasticity controls cell proliferation, surface marker expression and motile phenotype in amniotic fluid-derived stem cells, *J. Mech. Behav. Biomed. Mater.*, 2013, **17**, 307–316.
38 A. J. Engler, S. Sen, H. L. Sweeney and D. E. Discher, Matrix Elasticity Directs Stem Cell Lineage Specification, *Cell*, 2006, **126**, 677–689.
39 S. Bäckström, J. Benavente, W. R. Berg, K. S. Stibius, M. Larsen, H. Bohr, *et al.*, Tailoring Properties of Biocompatible PEG-DMA Hydrogels with UV Light, *Mater. Sci. Appl.*, 2012, **03**, 425–431.
40 M. De Veij, P. Vandenabeele, T. De Beer, J. P. Remon and L. Moens, Reference database of Raman spectra of pharmaceutical excipients, *J. Raman Spectrosc.*, 2009, **40**, 297–307.
41 J. B. Lambert, S. Gronert, H. F. Shurvell and D. A. Lightner, in *Spektroskopie - Strukturaufklärung in der Organischen Chemie*, Pearson, 1st edn, 2012.
42 A. Ovsianikov, M. Malinauskas, S. Schlie, B. Chichkov, S. Gittard, R. Narayan, *et al.*, Three-dimensional laser micro- and nano-structuring of acrylated poly(ethylene glycol) materials and evaluation of their cytoxicity for tissue engineering applications, *Acta Biomater.*, 2011, **7**, 967–974.
43 X. Gong, J. Yao, H. He, X. Zhao, X. Liu, F. Zhao, *et al.*, Combination of flow and micropattern alignment affecting flow-resistant endothelial cell adhesion, *J. Mech. Behav. Biomed. Mater.*, 2017, **74**, 11–20.
44 Y. Sun, R. Duffy, A. Lee and A. W. Feinberg, Optimizing the structure and contractility of engineered skeletal muscle thin films, *Acta Biomater.*, 2013, **9**, 7885–7894.
45 B. Zeng, Z. Cai, J. Lalevée, *et al.*, Cytotoxic and cytocompatible comparison among seven photoinitiators-triggered polymers in different tissue cells, *Toxicol. In Vitro*, 2021, **72**, 105103.

